JACS Au
AN OPEN ACCESS JOURNAL OF THE AMERICAN CHEMICAL SOCIETY

Open Access
This article is licensed under CC-BY-NC-ND 4.0

pubs.acs.org/jacsau
Letter

The Mononuclear Metal-Binding Site of Mo-Nitrogenase Is Not Required for Activity

Cécile Cadoux,[†] Nevena Maslać,[†] Léa Di Luzio, Daniel Ratcliff, Wenyu Gu, Tristan Wagner,* and Ross D. Milton*

Cite This: *JACS Au* 2023, 3, 2993−2999
Read Online

ACCESS | Metrics & More | Article Recommendations | Supporting Information

ABSTRACT: The biological N_2-fixation process is catalyzed exclusively by metallocofactor-containing nitrogenases. Structural and spectroscopic studies highlighted the presence of an additional mononuclear metal-binding (MMB) site, which can coordinate Fe in addition to the two metallocofactors required for the reaction. This MMB site is located 15-Å from the active site, at the interface of two NifK subunits. The enigmatic function of the MMB site and its implications for metallocofactor installation, catalysis, electron transfer, or structural stability are investigated in this work. The axial ligands coordinating the additional Fe are almost universally conserved in Mo-nitrogenases, but a detailed observation of the available structures indicates a variation in occupancy or a metal substitution. A nitrogenase variant in which the MMB is disrupted was generated and characterized by X-ray crystallography, biochemistry, and enzymology. The crystal structure refined to 1.55-Å revealed an unambiguous loss of the metal site, also confirmed by an absence of anomalous signal for Fe. The position of the surrounding side chains and the overall architecture are superposable with the wild-type structure. Accordingly, the biochemical and enzymatic properties of the variant are similar to those of the wild-type nitrogenase, indicating that the MMB does not impact nitrogenase's activity and stability *in vitro*.

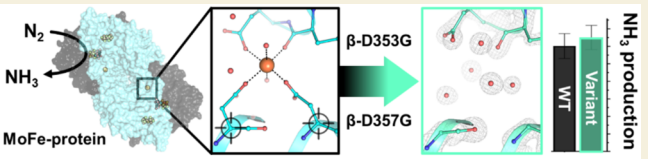

KEYWORDS: *Nitrogenase, X-ray crystallography, nitrogen fixation, cooperativity, FeS clusters*

Diazotrophic microbes exhibit the particularity of reducing dinitrogen (N_2) to ammonia (NH_3), a chemical reaction considered to be among the most challenging in biology due to the large activation energy (+251 kJ/mol) that must be surmounted.[1] Instead of activating the triple-bond of N_2 with high temperature and pressure, as in the Haber−Bosch process, microbes rely on energy released by the hydrolysis of adenosine triphosphate (ATP). In Mo-dependent nitrogenase, this reaction requires the hydrolysis of a minimum of 16 ATPs to reduce each N_2 to NH_3, with an approximate second-order rate constant (k_{cat}/K_m) of ~10^4 M^{-1} s^{-1}.[2−7] Mo-nitrogenase consists of two components, *(i)* the homodimeric Fe protein that transfers an electron of low-potential concomitantly with ATP-hydrolysis and *(ii)* the $\alpha_2\beta_2$ heterotetrameric MoFe protein harboring the P cluster (a [8Fe-7S] cluster) and the FeMo-cofactor (a [7Fe-Mo-9S-C] cluster bound to homocitrate) where N_2 is reduced (Figure 1A−C). The catalytic mechanism of the reaction has been studied for decades, revealing the complex ballet between the association of the Fe protein to the MoFe protein for electron transfer and FeMo-cofactor reactivity. Importantly, cooperativity is observed between each P cluster/FeMo cofactor-containing $\alpha\beta$ half of the MoFe protein during turnover.[8−10] Recently, structural investigation by cryo-electron microscopy also highlighted the asymmetry of Fe protein association to the MoFe protein and its impact on local rearrangement close to the catalytic center.[11]

While the P cluster and FeMo cofactor have attracted much attention, an additional Fe atom has been discovered at the $\beta\beta'$ junction of the MoFe protein (the prime indicates the second protomer of the dimer, Figure 1A) close to the surface of the protein. Atomic resolution X-ray crystallography combined with anomalous information and spectroscopic analyses confirmed the identity of the metal in a ferrous (Fe^{2+}) oxidation state. The Fe has a partial occupancy, which might explain why it was mostly modeled as calcium or magnesium in previous structural work (Supporting Information Table S2).[12] Since other cations might be bound to the site, the abbreviation MMB (mononuclear metal-binding) site was adopted.

This MMB site is flanked by three carboxy groups (β-E109, ß′-D353, and β'-D357, using nomenclature from the MoFe protein of *Azotobacter vinelandii*), a main chain carbonyl (β-R108), and two aqua ligands, yielding approximate octahedral coordination geometry (Figure 1D). In *Bacteria*, β-D353, β-D357, and β-E109 are all perfectly conserved across 255 sequences after filtering (described in the Materials and

Received: September 26, 2023
Revised: October 23, 2023
Accepted: October 23, 2023
Published: November 6, 2023

ACS Publications
© 2023 The Authors. Published by American Chemical Society

https://doi.org/10.1021/jacsau.3c00567
JACS Au 2023, 3, 2993−2999

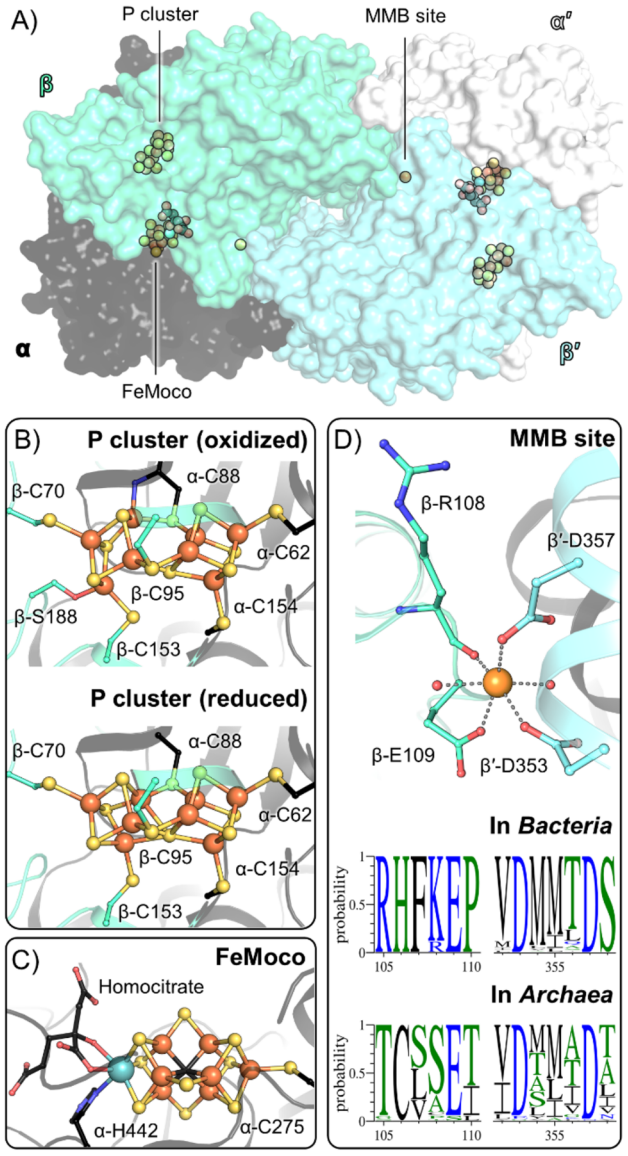

Figure 1. (A) Overall organization of the MoFe protein, based on the atomic resolution model (PDB 3U7Q), and (B and C) composition of its metallocofactors. (D) Organization and conservation of the MMB site in nitrogenases. The calcium atom modeled in the structure of PDB 3U7Q was exchanged by a Fe based on PDB 4TKU. Fe, S, and Mo are shown as spheres and colored as orange, yellow, and cyan, respectively. The FeMo cofactor is abbreviated as FeMoco.

Methods). In *Archaea*, these three residues are mostly conserved, and only a few sequences present substitutions (see Supporting Information). β-R108 is not conserved in either group, possibly because it provides coordination through the peptide backbone (Figure 1D).[12] They are also conserved in the sequences of the V and Fe isoforms, in the phylogenetically distant *Methanococcales* and *Methanobacteriales* sequences, and even in the BchNB protein of the homologous dark operative protochlorophyllide oxidoreductase.[12−15]

Despite its conservation, the possible importance of the MMB and potentially coordinated Fe has not been determined in nitrogenases. We hypothesized that it could be involved in optimizing the loading of the metallocofactors in the enzyme, catalytic efficiency, structural stability, or electron transfer. For instance, the homologous position of the Asp357 found in BchNB facilitates proton transfer during protochlorophyllide reduction.[16] Herein, we created a MoFe protein variant lacking key metal-coordinating residues to investigate the functional importance of the MMB through structural and biochemical characterization.

Metal coordination at the MMB site was disrupted by substituting aspartates β-D353/D357 with glycine residues in *Azotobacter vinelandii* DJ by homologous double-reciprocal recombination.[8] Anoxic purification of the generated β-D353G/D357G MoFe variant (via affinity, anion exchange, and size-exclusion chromatography, Figure S1) yielded exploitable crystals belonging to the monoclinic *C*2 space group and containing an $\alpha_2\beta_2$ heterotetramer in the asymmetric unit (Figure 2A, Table S3). The structure, refined to 1.55-Å resolution, has the typical MoFe-protein organization with an excellent fit to the previously characterized atomic resolution model (root-mean-square deviation of 0.235-Å for 1858 Cα atoms when aligned to PDB 3U7Q, Figure 2A). The

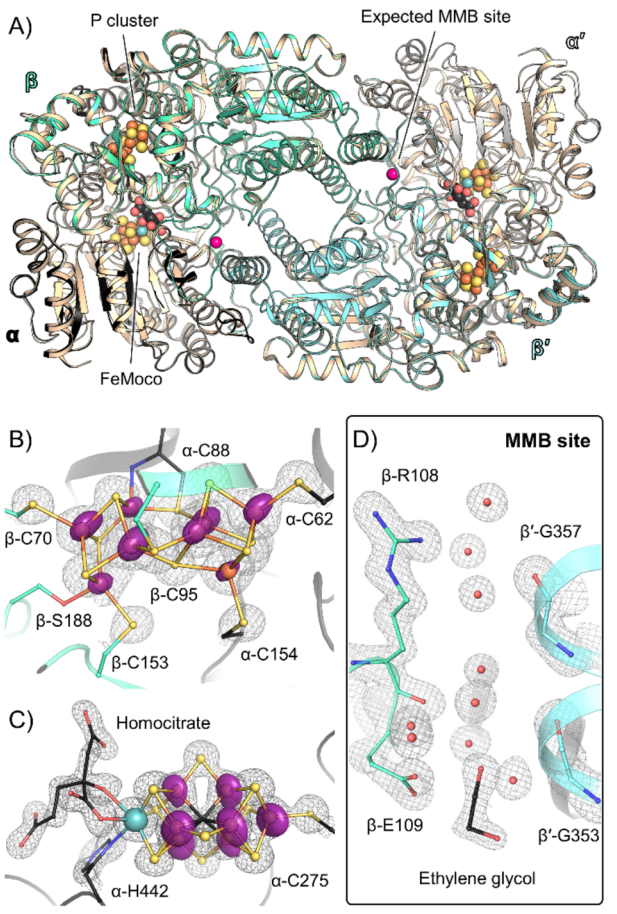

Figure 2. (A) Overlay of the β-D353G/D357G variant with the wild-type MoFe protein (PDB 3U7Q, colored in wheat). (B−D) Close-up of the P cluster, with only the oxidized state shown for clarity (B), the FeMo cofactor (C), and the MMB site (D). The protein is shown as transparent cartoons, and residues/metals as balls and sticks. In panels (B) and (C) the $2F_o - F_c$ electron density (black mesh) and the anomalous (transparent purple surface) maps are contoured at 2.5σ and 10σ, respectively. In panel (D), the $2F_o - F_c$ electron density map is contoured at 1.5σ, and no peaks can be detected in the anomalous map at this site.

https://doi.org/10.1021/jacsau.3c00567
JACS Au 2023, 3, 2993−2999

slight deviation observed at the periphery is most likely due to the difference in the crystal packing (Figure S2).

The electron density profile presents a fully occupied P cluster, which fits with a mixture of oxidized and reduced states modeled at 90 and 10% occupancy, respectively (Figure 2B and Figure S3). The FeMo cofactor also presents perfect integrity and occupies the active site at full occupancy (Figure 2C). Both metallocofactors share identical atomic positions compared to the previously described structures (Figures S3 and S4), with the Fe position corroborated by an anomalous signal (Figures 2B and 2C).

As expected, the MMB site is vacant in the created β-D353G/D357G variant and is filled with water and an ethylene glycol molecule (Figure 2D). The modeled ethylene glycol presence suggests that the MMB site is not isolated from the solvent, explaining why Fe can be exchanged for other cations (*e.g.*, Ca^{2+}) or diffuse out of this site. Accordingly, no anomalous signal could be detected in this area. The β-G353 and β-G357 atomic positions overlay the main chain of the structures containing a partially modeled ion (Figure S5). The close environment, in particular the positions of β-E109 and β-R108, is equivalent to that of the wild-type. Deficiency in the MMB site does not impact the structural integrity of the two other metallocofactors and the overall structure; however, the crystal packing may hide unsuspected features compared with the protein behavior in solution (*i.e.*, protein dynamics during turnover).

The generated *A. vinelandii* mutant strain retained its diazotrophic phenotype (Figure S6), providing an initial indication that disruption of the MMB site did not abolish nitrogenase's N_2 fixation activity. *In vitro* activity assays were performed for *(i)* H_2 production under Ar and *(ii)* H_2/NH_3 production under N_2 (Figure 3). The β-D353G/D357G MoFe protein remains fully active and presents specific activities equivalent to the wild-type MoFe protein under these conditions. The determined catalytic parameters confirmed that the mutant MoFe protein exhibits similar affinity towards N_2 as the wild-type MoFe protein.[8,17]

The electron distribution toward NH_3 was found to be ~60% under both low-flux (4 mol equiv of Fe protein per MoFe protein) and high-flux (16 mol equiv of Fe per MoFe) turnover conditions, suggesting that the MMB site does not impact the selectivity of nitrogenase toward N_2 under these *in vitro* conditions (Figure S7).

The intrinsic dynamics of the β-D353G/D357G MoFe protein was also probed by size exclusion chromatography (Figure S8) and limited proteolysis (Figure S9). In both experiments, the β-D353G/D357G variant and the wild-type showed a similar profile, corroborating the structural analysis. The melting temperature of the two MoFe proteins was determined by circular dichroism to be ~57 °C in both cases, confirming that the presence of the MMB site also does not introduce a pronounced stabilizing effect on the total secondary structure of the MoFe protein (Figure S10).[18]

Finally, protein−protein associations with this β-D353G/D357G MoFe protein were investigated further by considering protein-mediated protection of nitrogenase against oxidative damage in the obligate aerobe *A. vinelandii*. In the presence of molecular oxygen (O_2), the Fe and MoFe proteins form a tripartite complex with a small ferredoxin-like protein ("FeSII" or "Shethna" protein) that restricts access of O_2 to its metallocofactors (*i.e.*, a switch-off protection mechanism).[19,20] All three components are essential for this protection

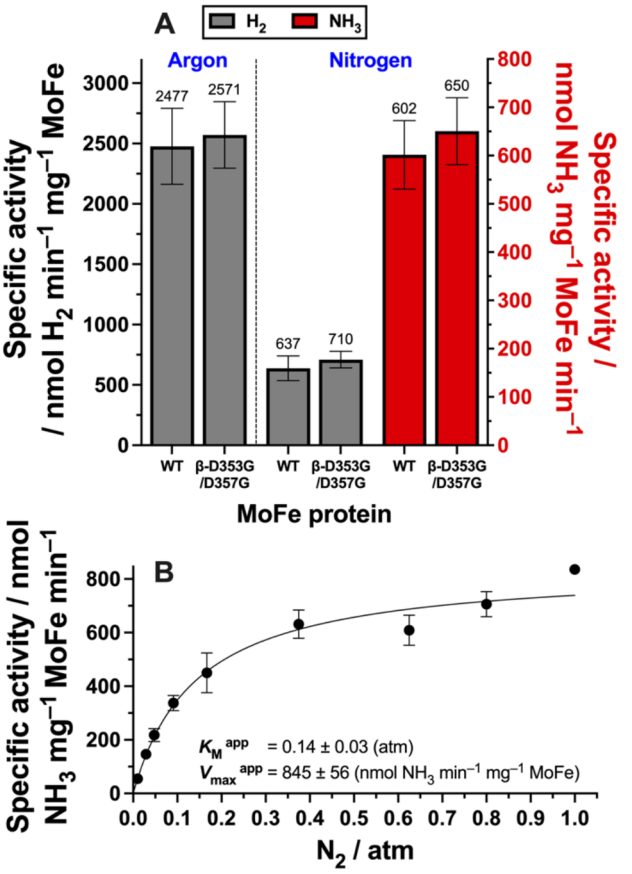

Figure 3. (A) Specific activities of wild-type (WT) and β-D353G/D357G MoFe for H_2 and NH_3 production during turnover under Ar or N_2 (1 atm). Assays were performed using three biological replicates of each MoFe protein. For technical repeats $n = 3$. (B) Representative apparent Michaelis−Menten kinetic parameters for the β-D353G/D357G MoFe protein. All assays were performed at 30 °C for 8 min and contained 0.1 mg of MoFe protein with 16 mol equiv of Fe protein. Sample quantification and additional assay information can be found in the Supporting Information. $n = 3$, and $n = 2$ for the 1 atm N_2 data point in (B).

mechanism. As presented in Figure S11A (Supporting Information), 66% of nitrogenase H_2-formation activity (1 atm Ar atmosphere) could be preserved during exposure to 2% O_2 (for 10 min) when the wild-type MoFe protein was used. Importantly, only 16% of the activity could be preserved in the case of the β-D353G/D357G MoFe protein. These data suggest that the MMB site may indeed play a non-negligible role in nitrogenase catalysis *in vitro*, and possibly, *in vivo*. However, this difference was not observed when performed under 1 atm of N_2 where H_2 and NH_3 production was quantified (Figure S11B, Supporting Information). This may be due to a difference in reaction mechanism for H_2 formation *versus* N_2 fixation, although concrete interpretation is complicated by the difference in total electron flux observed for nitrogenase when solely producing H_2 and not fixing N_2. Further extensive investigation is required to better understand the interaction between the β-D353G/D357G MoFe protein and the Fe/FeSII proteins during protection from O_2 deactivation.[8]

In conclusion, our study suggests that the MMB site is not involved in the P-cluster and FeMo cofactor installation, as both metallocofactors exhibit full occupancy and appropriate

https://doi.org/10.1021/jacsau.3c00567
JACS Au 2023, 3, 2993−2999

coordination. Nitrogenase's overall dynamic and N_2-fixation capabilities are also not impacted by the MMB site absence, even when assayed at the physiological temperature of 30 °C *in vitro*. Such an observation is in accordance with numerous structural works, which showed that an absence of Fe switches the side chain of β-E109 without impacting the surrounding residues (Table S1). The structural similarity between the wild-type and the presented β-D353G/D357G variant might be due to a crystallographic artifact in which the crystal packing rigidified a particular state allowing the partial release of the MMB without affecting the structure (Figure S2). Different cryo-electron microscopy snapshots recorded under turnover conditions present the additional electron density for the MMB; interestingly, the MMB site observed in the various trapped structures displays the same architecture (Figure S12), as well as its surrounding, reinforcing the concept that the site is not involved in the catalytic turnover. Nevertheless, we cannot exclude that the MMB site might influence a fine-tuning of the overall N_2-fixation process by optimizing the asymmetry dynamics between the Fe protein and the MoFe protein or the cooperativity between the subunits.[8]

MATERIALS AND METHODS

In Silico Analysis

The sequence logos[21] were created using the WebLogo 3 server.[22] The homologous sequences used for the logos were obtained by BlastP[23] search in the RefSeq Select database[24] against *A. vinelandii* DJ NifK (NCBI accession number WP_012698833.1) with default parameters. The 250 closest homologues were filtered for redundancy and manually checked for correct annotation. The final data set after filtering consisted of 225 bacterial and 55 archaeal sequences (accession numbers for all used sequences can be found in Supplementary Table S4). The alignment used as an input for sequence logo generation was done using the MUSCLE server.[25]

A. vinelandii Cultures and Media

The procedure is outlined in the Supporting Information and was developed previously with minor modifications.[8]

Preparation of the *A. vinelandii* Strain Producing β-D353G/D357G MoFe Protein

The β-D353G/D357G MoFe mutant was created using the double homologous recombination method as previously described[8] and is detailed in the Supporting Information.

Purification of Wild-Type, β-D353G/D357G MoFe Protein, and Fe Protein

The procedures outlined here were developed previously with minor modifications[8] and are extensively detailed in the Supporting Information.

Activity Assays

Activity assays were performed as recently reported.[8] Substrate reduction activity assays were conducted in triplicate (except where explicitly stated) 1 mL reactions in 13 mL septum-sealed glass vials (Wheaton) containing deoxygenated buffer and an ATP-regenerating system (5 mM ATP, 30 mM phosphocreatine, 1.3 mg of Bovine Serum Albumin, 0.2 mg of creatine phosphokinase (from Rabbit muscle, Merck Switzerland), 10 mM sodium dithionite, and 100 mM MOPS/NaOH at pH 7.0). Activity assays contained 0.1 mg of MoFe protein and either 16.6 mol equiv of Fe protein (0.5 mg, "high-flux") or 4 mol equiv of Fe protein (0.12 mg, "low-flux"). All reaction vials were sealed within an Ar-filled glovebox (Jacomex, France) and vented to atmospheric pressure. Where necessary, vials were flushed with ultra-high-purity N_2 (or desired quantities were introduced using gastight syringes); all vials were vented to atmospheric pressure before reactions were initiated. Reactions were performed within a shaking water bath (30 °C) and initiated by the addition of $MgCl_2$ (from a 1 M stock, 10 mM final concentration) using a gastight syringe. Reactions were quenched after 8 min by the addition of 300 μL of 400 mM EDTA (pH 8.0). H_2 quantification was performed on all reactions using a calibrated GC-TCD equipped with a 5 Å molecular sieve column (Ar carrier, SRI Instruments model 8610C). Ammonia was quantified by the *o*-phthalaldehyde method (corrected to controls and assays performed under 1 atm Ar) using NH_4Cl as the standard, as reported previously.[26,27]

O_2 Protection Assays

Activity assays were performed using the "FeSII" (or "Shethna") protein of *A. vinelandii*, heterologously produced in *E. coli*. The protein was expressed and purified as previously published, with a single modification: in this work, the gene corresponding to the FeSII protein was introduced to a pET21a vector (Merck Millipore).[28] The ability of the FeSII protein to protect nitrogenase from oxidation by O_2 was determined based on the quantity of H_2 and/or NH_3 produced in a nitrogenase assay following exposure to O_2 for 10 min. Assays employed the same buffer components as listed above, except that DT was omitted and $MgCl_2$ (10 mM) was included in the activity assay buffer. All protein components (when used) were present at an equimolar concentration for these assays (either 0.4 or 1.2 μM, as stated in the Figure S11 caption). All reaction vials were first assembled within an Ar-filled glovebox (Jacomex, France) and vented to atmospheric pressure. Where necessary, vial headspaces were replaced with 1 atm of 5.0 N_2 gas by vacuum-flushing cycles on a homemade system. When required, O_2 (final concentration of 2% v/v) was added using gastight syringes, and the vials were incubated for 10 min at 30 °C. Vials were then flushed with ultra-high purity Ar or N_2 gas (5.0, consisting of 3 x vacuum/flushing cycles). All reaction vials were once again vented to atmospheric pressure. Reactions were performed in a shaking water bath (30 °C) and initiated by the addition of sodium dithionite (from a 1 M stock, 20 mM final concentration) using a gastight syringe. Reactions were quenched after 8 min by the addition of 300 μL of 400 mM EDTA (pH 8.0). H_2 was quantified by GC-TCD (using a molecular sieve 5 Å column with Ar carrier gas, SRI Instruments USA model 8610C), and NH_3 was quantified by fluorescence using the OPA method, as described above.[8]

Analytical Gel Filtration

Analytical gel filtration was performed using an Äkta Go within an anoxic glovebox.[8] The proteins were diluted with the running buffer (50 mM Tris/HCl, 500 mM NaCl, pH 8, 0.5 mM DT) to a concentration of 17 nmol/mL for MoFe protein. 200 μL aliquots were prepared and incubated for 1 h before being loaded (100 μL) onto the pre-equilibrated column.

Limited Proteolysis

A 50 mM Tris/HCl (pH 7.6) buffer containing 10 mM $CaCl_2$ was prepared and deoxygenated in an Ar-filled glovebox (Jacomex, France) overnight. The buffer was split into 2

https://doi.org/10.1021/jacsau.3c00567
JACS Au 2023, 3, 2993−2999

bottles, and 0.2 mg/mL fresh trypsin (Sigma) was added to the first. This trypsin-containing buffer was then activated at 30 °C for 20 min using a heating block. Proteins were brought into the glovebox and diluted to a concentration of 1 mg/mL using the buffer that did not contain trypsin. The proteins were placed in LC/MS vials with stirring in a water bath at 37 °C, and the activated trypsin was then added to the protein samples to a final concentration of 2 μg/mL trypsin (final ratio of 500:1 MoFe:trypsin) as the starting point for the reaction.

The protein reactions were sampled at time 0 (before trypsin addition), 2, 5, 30, 60, and 90 min after trypsin addition. 4 μL of samples of the reactions were transferred to Eppendorf tubes that already contained 4 μL of TruPAGE LDS (4×) sample buffer (Merck, Switzerland) and then immediately placed at 95 °C on a heating block for 5 min to deactivate the trypsin and terminate proteolysis. 1.6 μL of 1 M dithiothreitol (DTT) and 6.4 μL of MilliQ water were added afterward. 4-20% mPAGE Bis-tris gels (Merck, Switzerland) were used for analysis. 7-μL aliquots of the treated protein samples were loaded in each well (1.75 μg MoFe protein). The gel was run at 200 V and stained with One-Step Blue (Biotium, Brunschwig Switzerland).

Circular Dichroism

All circular dichroism experiments were performed using a sealed cuvette with a 1-mm path length. The anoxic protein samples were loaded in the cuvette within an anoxic glovebox (Ar atmosphere, <1 ppm O_2). Protein samples were diluted to 0.2 mg/mL in 50 mM Tris/HCl, 0.5 M NaCl pH 8.0 buffer. Circular dichroism spectra were recorded first to determine lambda max (224 nm for both MoFe proteins). For the melting point experiments, the temperature was ramped 1 °C per minute starting from 20 to 80 °C. Reactions were conducted in triplicate for both MoFe proteins.

Crystallization of the β-D353G/D357G MoFe Protein

The β-D353G/D357G MoFe protein was crystallized anaerobically at 17.5 mg/mL^{-1} under a 100% N_2 atmosphere using the OryxNano Crystallization Robot (Douglas Instruments Ltd., Berkshire, United Kingdom). Prior to crystallization, the sample was centrifuged at 13,000 *x g* for 3 min to remove macroaggregates and dust. The protein was spotted as a sitting drop to 96-Well MRC 2-Drop polystyrene crystallization plates (SWISSCI) containing 90 μL of crystallization solution in the reservoir. The following crystallization screens were used to harvest crystals JCSG++, XP Screen, PEP, Wizard 1/2, Wizard 3/4, and PACT++ (Jena Bioscience, Germany). Each drop contained 0.5 μL of protein sample and 0.5 μL of crystallization solution. Crystals were obtained in the crystallization solution containing 10% w/v polyethylene glycol 10,000, 2% v/v 1,4-dioxane, 100 mM trisodium citrate; pH 5.6, and 1 mM polyoxotungstate $[TeW_6O_{24}]^{6-}$ (TEW). Sealed plates were stored inside a Coy anaerobic chamber (Coy Laboratory Products Inc., Grass Lake, USA) with an atmosphere of N_2:H_2 97:3 at 20 °C. Crystals were soaked in the crystallization solution supplemented with 30% v/v ethylene glycol for a few seconds before freezing in liquid nitrogen.

Data Processing and Refinement

Crystals were tested and collected at 100 K at the Swiss Light Source X06DA (Villigen, Switzerland). Data sets were collected at 1.73648-Å (7,140 eV) for the single-wavelength anomalous dispersion experiment. It must be specified here that the presence of Fe at this MMB site has an absorption edge 5 eV higher in comparison to the Fe atoms composing the two other metallocofactors, and the data presented here were collected at an energy of 7,140 eV for this purpose (the theoretical absorption of Fe at its K-edge is 7,112 eV).[12] Native data sets were collected at a wavelength of 1.00002-Å on the same crystal. Data were processed with *autoPROC* run with staraniso due to the high anisotropy.[29] For the Fe-K edge data set, the diffraction limits along the principal axes are the following: a = 2.43 Å, b = 2.27 Å, and c = 1.67 Å. For the data set collected close to the Se K edge, the diffraction limits along the principal axes are the following: a = 2.33 Å, b = 2.04 Å, and c = 1.53 Å. The structure of the variant was solved by using *PHENIX* with the following template: 3U7Q. The model was manually rebuilt with *COOT* and further refined with *PHENIX*.[30] During the refinement, a translational-libration screw was applied with the model containing hydrogens added in the riding position during the last refinement cycles. Hydrogens were removed in the final deposited model. The model was validated through the MolProbity server.[31] Data collection and refinement statistics for the deposited model and structure factors are listed in Table S3. The model is accessible via PDB ID 8P8G. Figures were generated with PyMOL (Schrödinger, LLC).

■ ASSOCIATED CONTENT

Data Availability Statement

Raw data are freely available on the Zenodo repository: 10.5281/zenodo.7973626.

Supporting Information

The Supporting Information is available free of charge at https://pubs.acs.org/doi/10.1021/jacsau.3c00567.

Experimental details about the strategy used to generate the *A. vinelandii* DJ strain derivative producing β-D353G/D357G MoFe protein and *A. vinelandii* culture and media; comparison of MMB site occupancy in deposited structures; X-ray analysis statistics for the presented structure; accession numbers for sequences used in conservation analysis; SDS-PAGE and native-PAGE analysis of the wild-type and β-D353G/D357G MoFe proteins (PDF)

■ AUTHOR INFORMATION

Corresponding Authors

Ross D. Milton − *Department of Inorganic and Analytical Chemistry, Faculty of Sciences and National Centre of Competence in Research (NCCR) Catalysis, University of Geneva, 1211 Geneva 4, Switzerland;* orcid.org/0000-0002-2229-0243; Email: ross.milton@unige.ch

Tristan Wagner − *Max Planck Institute for Marine Microbiology, 28359 Bremen, Germany;* orcid.org/0000-0002-3382-8969; Email: twagner@mpi-bremen.de

Authors

Cécile Cadoux − *Department of Inorganic and Analytical Chemistry, Faculty of Sciences and National Centre of Competence in Research (NCCR) Catalysis, University of Geneva, 1211 Geneva 4, Switzerland*

Nevena Maslać − *Max Planck Institute for Marine Microbiology, 28359 Bremen, Germany*

https://doi.org/10.1021/jacsau.3c00567
JACS Au 2023, 3, 2993−2999

Léa Di Luzio − *Department of Inorganic and Analytical Chemistry, Faculty of Sciences, University of Geneva, 1211 Geneva 4, Switzerland*

Daniel Ratcliff − *Department of Inorganic and Analytical Chemistry, Faculty of Sciences and National Centre of Competence in Research (NCCR) Catalysis, University of Geneva, 1211 Geneva 4, Switzerland*

Wenyu Gu − *Laboratory of Microbial Physiology and Resource Biorecovery, School of Architecture, Civil and Environmental Engineering (ENAC), École Polytechnique Fédérale de Lausanne (EPFL), CH-1015 Lausanne, Switzerland*

Complete contact information is available at: https://pubs.acs.org/10.1021/jacsau.3c00567

Author Contributions

†C.C. and N.M. contributed equally. C.C., W.G., and R.D.M. designed the research. C.C., L.D.L., W.G., and R.D.M. constructed and produced the β-D353G/D357G MoFe protein mutant. C.C. performed limited proteolysis; and C.C., L.D.L., and D.R. performed activity assays. N.M. performed the crystallization. X-ray data collection was performed by N.M. and T.W. Data processing, model building, structure refinement, validation, and deposition were performed by N.M. and T.W. Structures were analyzed by N.M. and T.W. N.M. performed the sequence comparison analyses. R.D.M. and T.W. acquired funding to realize the project. The manuscript was written through contributions of all authors. All authors have given approval to the final version of the manuscript. CRediT: **Cécile Cadoux** conceptualization, data curation, formal analysis, investigation, methodology, supervision, validation, writing-original draft, writing-review & editing; **Nevena Maslać** conceptualization, data curation, formal analysis, investigation, methodology, validation, visualization, writing-original draft, writing-review & editing; **Léa Di-Luzio** data curation, formal analysis, investigation, writing-original draft, writing-review & editing; **Daniel Ratcliff** conceptualization, data curation, formal analysis, investigation, methodology, supervision, validation, writing-original draft, writing-review & editing; **Wenyu Gu** conceptualization, data curation, formal analysis, investigation, methodology, validation, writing-original draft, writing-review & editing; **Tristan Wagner** conceptualization, data curation, formal analysis, funding acquisition, investigation, methodology, project administration, resources, software, supervision, validation, visualization, writing-original draft, writing-review & editing; **Ross D. Milton** conceptualization, data curation, formal analysis, funding acquisition, investigation, methodology, project administration, resources, software, supervision, validation, visualization, writing-original draft, writing-review & editing.

Funding

This study was funded by the Max Planck Society for T.W. and N.M. T.W. was supported by the Deutsche Forschungsgemeinschaft Schwerpunktprogram 1927 “Iron-sulfur for Life” (WA 4053/1-1). This publication was created as part of NCCR Catalysis (grant number 180544), a National Centre of Competence in Research funded by the Swiss National Science Foundation.

Notes

The authors declare no competing financial interest.

ACKNOWLEDGMENTS

We thank the Max Planck Institute for Marine Microbiology for continuous support. We acknowledge the Swiss light Source Synchrotron for the beamtime and especially the staff of beamline X06DA. We would like to thank Ramona Appel and Christina Probian for their continuous support in the Microbial Metabolism laboratory. We thank Gloria Sedoh, Plinio Maroni, Olivier Vassalli, Naomi Sakai, Isabelle Worms and the staff of the Department of Inorganic and Analytical Chemistry (UNIGE) for experimental and technical support.

ABBREVIATIONS

ATP, adenosine triphosphate; MMB site, mononuclear metal binding site

REFERENCES

(1) Mus, F.; Alleman, A. B.; Pence, N.; Seefeldt, L. C.; Peters, J. W. Exploring the alternatives of biological nitrogen fixation. *Metallomics* **2018**, *10* (4), 523−538.

(2) Burén, S.; Jiménez-Vicente, E.; Echavarri-Erasun, C.; Rubio, L. M. Biosynthesis of Nitrogenase Cofactors. *Chemical Reviews* **2020**, *120* (12), 4921−4968.

(3) Einsle, O.; Rees, D. C. Structural Enzymology of Nitrogenase Enzymes. *Chemical Reviews* **2020**, *120* (12), 4969−5004.

(4) Jasniewski, A. J.; Lee, C. C.; Ribbe, M. W.; Ribbe, M. W.; Hu, Y. Reactivity, Mechanism, and Assembly of the Alternative Nitrogenases. *Chemical Reviews* **2020**, *120* (12), 5107−5157.

(5) Rutledge, H. L.; Tezcan, F. A. Electron Transfer in Nitrogenase. *Chemical Reviews* **2020**, *120* (12), 5158−5193.

(6) Seefeldt, L. C.; Yang, Z. Y.; Lukoyanov, D. A.; Harris, D. F.; Dean, D. R.; Raugei, S.; Hoffman, B. M. Reduction of Substrates by Nitrogenases. *Chemical Reviews* **2020**, *120* (12), 5082−5106.

(7) Van Stappen, C.; Decamps, L.; Cutsail, G. E.; Bjornsson, R.; Henthorn, J. T.; Birrell, J. A.; Debeer, S. The Spectroscopy of Nitrogenases. *Chemical Reviews* **2020**, *120* (12), 5005−5081.

(8) Cadoux, C.; Ratcliff, D.; Maslać, N.; Gu, W.; Tsakoumagkos, I.; Hoogendoorn, S.; Wagner, T.; Milton, R. D. Nitrogen Fixation and Hydrogen Evolution by Sterically Encumbered Mo-Nitrogenase. *JACS Au* **2023**, *3* (5), 1521−1533.

(9) Danyal, K.; Shaw, S.; Page, T. R.; Duval, S.; Horitani, M.; Marts, A. R.; Lukoyanov, D.; Dean, D. R.; Raugei, S.; Hoffman, B. M.; Seefeldt, L. C.; Antony, E. Negative cooperativity in the nitrogenase Fe protein electron delivery cycle. *Proceedings of the National Academy of Sciences* **2016**, *113* (40), E5783−E5791.

(10) Truscott, S.; Lewis, R. S.; Watt, G. D. Positive cooperativity during *Azotobacter vinelandii* nitrogenase-catalyzed acetylene reduction. *Biophysical Chemistry* **2021**, *277*, 106650−106650.

(11) Rutledge, H. L.; Cook, B. D.; Nguyen, H. P. M.; Herzik, M. A., Jr.; Tezcan, F. A. Structures of the nitrogenase complex prepared under catalytic turnover conditions. *Science* **2022**, *377* (6608), 865−869.

(12) Zhang, L.; Kaiser, J. T.; Meloni, G.; Yang, K.-Y.; Spatzal, T.; Andrade, S. L. A.; Einsle, O.; Howard, J. B.; Rees, D. C. The Sixteenth Iron in the Nitrogenase MoFe Protein. *Angewandte Chemie International Edition* **2013**, *52* (40), 10529−10532.

(13) Bröcker, M. J.; Schomburg, S.; Heinz, D. W.; Jahn, D.; Schubert, W.-D.; Moser, J. Crystal Structure of the Nitrogenase-like Dark Operative Protochlorophyllide Oxidoreductase Catalytic Complex $(ChlN/ChlB)_2$. *J. Biol. Chem.* **2010**, *285* (35), 27336−27345.

(14) Boyd, E. S.; Hamilton, T. L.; Peters, J. W. An alternative path for the evolution of biological nitrogen fixation. *Front Microbiol* **2011**, *2* (OCT), 1−11.

(15) Maslać, N.; Sidhu, C.; Teeling, H.; Wagner, T. Comparative Transcriptomics Sheds Light on Remodeling of Gene Expression during Diazotrophy in the Thermophilic Methanogen *Methanothermococcus thermolithotrophicus*. *mBio* **2022**, *13* (6), e02443-22.

(16) Muraki, N.; Nomata, J.; Ebata, K.; Mizoguchi, T.; Shiba, T.; Tamiaki, H.; Kurisu, G.; Fujita, Y. X-ray crystal structure of the light-independent protochlorophyllide reductase. *Nature* **2010**, *465* (7294), 110−4.
(17) Harris, D. F.; Lukoyanov, D. A.; Shaw, S.; Compton, P.; Tokmina-Lukaszewska, M.; Bothner, B.; Kelleher, N.; Dean, D. R.; Hoffman, B. M.; Seefeldt, L. C. Mechanism of N_2 Reduction Catalyzed by Fe-Nitrogenase Involves Reductive Elimination of H_2. *Biochemistry* **2018**, *57* (5), 701−710.
(18) Greenfield, N. J. Using circular dichroism spectra to estimate protein secondary structure. *Nature Protocols* **2006**, *1* (6), 2876−2890.
(19) Shethna, Y. I.; DerVartanian, D. V.; Beinert, H. Non heme (iron-sulfur) proteins of *Azotobacter vinelandii*. *Biochem. Biophys. Res. Commun.* **1968**, *31* (6), 862−8.
(20) Schlesier, J.; Rohde, M.; Gerhardt, S.; Einsle, O. A Conformational Switch Triggers Nitrogenase Protection from Oxygen Damage by Shethna Protein II (FeSII). *J. Am. Chem. Soc.* **2016**, *138* (1), 239−247.
(21) Schneider, T. D.; Stephens, R. M. Sequence logos: a new way to display consensus sequences. *Nucleic Acids Res.* **1990**, *18* (20), 6097−100.
(22) Crooks, G. E.; Hon, G.; Chandonia, J. M.; Brenner, S. E. WebLogo: a sequence logo generator. *Genome Res.* **2004**, *14* (6), 1188−90.
(23) Altschul, S. F.; Gish, W.; Miller, W.; Myers, E. W.; Lipman, D. J. Basic local alignment search tool. *J. Mol. Biol.* **1990**, *215* (3), 403−10.
(24) O'Leary, N. A.; Wright, M. W.; Brister, J. R.; Ciufo, S.; Haddad, D.; McVeigh, R.; Rajput, B.; Robbertse, B.; Smith-White, B.; Ako-Adjei, D.; Astashyn, A.; Badretdin, A.; Bao, Y.; Blinkova, O.; Brover, V.; Chetvernin, V.; Choi, J.; Cox, E.; Ermolaeva, O.; Farrell, C. M.; Goldfarb, T.; Gupta, T.; Haft, D.; Hatcher, E.; Hlavina, W.; Joardar, V. S.; Kodali, V. K.; Li, W.; Maglott, D.; Masterson, P.; McGarvey, K. M.; Murphy, M. R.; O'Neill, K.; Pujar, S.; Rangwala, S. H.; Rausch, D.; Riddick, L. D.; Schoch, C.; Shkeda, A.; Storz, S. S.; Sun, H.; Thibaud-Nissen, F.; Tolstoy, I.; Tully, R. E.; Vatsan, A. R.; Wallin, C.; Webb, D.; Wu, W.; Landrum, M. J.; Kimchi, A.; Tatusova, T.; DiCuccio, M.; Kitts, P.; Murphy, T. D.; Pruitt, K. D. Reference sequence (RefSeq) database at NCBI: current status, taxonomic expansion, and functional annotation. *Nucleic Acids Res.* **2016**, *44* (D1), D733−D745.
(25) Madeira, F.; Pearce, M.; Tivey, A. R. N.; Basutkar, P.; Lee, J.; Edbali, O.; Madhusoodanan, N.; Kolesnikov, A.; Lopez, R. Search and sequence analysis tools services from EMBL-EBI in 2022. *Nucleic acids research* **2022**, *50* (W1), W276−W279.
(26) Milton, R. D.; Cai, R.; Abdellaoui, S.; Leech, D.; De Lacey, A. L.; Pita, M.; Minteer, S. D. Bioelectrochemical Haber−Bosch Process: An Ammonia-Producing H_2/N_2 Fuel Cell. *Angewandte Chemie - International Edition* **2017**, *56* (10), 2680−2683.
(27) Milton, R. D.; Abdellaoui, S.; Khadka, N.; Dean, D. R.; Leech, D.; Seefeldt, L. C.; Minteer, S. D. Nitrogenase bioelectrocatalysis: Heterogeneous ammonia and hydrogen production by MoFe protein. *Energy and Environmental Science* **2016**, *9* (8), 2550−2554.
(28) Milton, R. D.; Cai, R.; Sahin, S.; Abdellaoui, S.; Alkotaini, B.; Leech, D.; Minteer, S. D. The In Vivo Potential-Regulated Protective Protein of Nitrogenase in *Azotobacter vinelandii* Supports Aerobic Bioelectrochemical Dinitrogen Reduction In Vitro. *J. Am. Chem. Soc.* **2017**, *139* (26), 9044−9052.
(29) Vonrhein, C.; Flensburg, C.; Keller, P.; Sharff, A.; Smart, O.; Paciorek, W.; Womack, T.; Bricogne, G. Data processing and analysis with the *autoPROC* toolbox. *Acta Crystallographica Section D* **2011**, *67* (4), 293−302.
(30) Liebschner, D.; Afonine, P. V.; Baker, M. L.; Bunkóczi, G.; Chen, V. B.; Croll, T. I.; Hintze, B.; Hung, L. W.; Jain, S.; McCoy, A. J.; Moriarty, N. W.; Oeffner, R. D.; Poon, B. K.; Prisant, M. G.; Read, R. J.; Richardson, J. S.; Richardson, D. C.; Sammito, M. D.; Sobolev, O. V.; Stockwell, D. H.; Terwilliger, T. C.; Urzhumtsev, A. G.; Videau, L. L.; Williams, C. J.; Adams, P. D. Macromolecular structure determination using X-rays, neutrons and electrons: recent developments in *Phenix*. *Acta Crystallogr D Struct Biol* **2019**, *75* (Pt 10), 861−877.
(31) Williams, C. J.; Headd, J. J.; Moriarty, N. W.; Prisant, M. G.; Videau, L. L.; Deis, L. N.; Verma, V.; Keedy, D. A.; Hintze, B. J.; Chen, V. B.; Jain, S.; Lewis, S. M.; Arendall, W. B., 3rd; Snoeyink, J.; Adams, P. D.; Lovell, S. C.; Richardson, J. S.; Richardson, D. C. MolProbity: More and better reference data for improved all-atom structure validation. *Protein Sci.* **2018**, *27* (1), 293−315.

https://doi.org/10.1021/jacsau.3c00567
JACS Au 2023, 3, 2993−2999